Improved Transmission Probabilities for the Neutron Transport Problem with the Method of Characteristics in APOLLO

François Févotte, Simone Santandrea and Richard Sanchez

Abstract. The Method of Characteristics is an efficient tool for the numerical solution of the neutron transport problem. In this paper, a novel technique for a better computation of transmission probabilities in the Method of Characteristics is discussed. The technique relies on a transverse quadrature that properly accounts for discontinuities along trajectories, and on the use of a sei-analytical formula for the transverse integration of the transmission probability.

The implementation of this new technique has proved successful, insofar as it requires a much larger tracking step (up to five times) than the regular Method of Characteristics to obtain a given accuracy for the reaction rates, as our numerical results show. A comparison of the agorithmic complexity suggests that the new method could lead to significant gains in terms of computing times (up to 30%). The new method also guarantees a monotonous convergence with respect to the transverse discretization.

Keywords

Neutron transport, numeric simulation, method of characteristics, tracking, transmission probabilities.

1. Introduction

At the various stages of a nuclear reactor's life, numerous studies are needed to guaranty the safety and efficiency of the design, analyse the fuel cycle, prepare the dismantlement, and so on. Due to the extreme difficulty (and in some cases, impossibility) to take extensive and accurate measurements in the reactor core, most of these studies are numerical simulations.

The complete numerical simulation of a nuclear reactor involves many types of physics: neutronics, thermal hydraulics, materials, control engineering, ...). It therefore requires complex simulation schemes involving various computing codes and coupling techniques. Among these, the neutron transport simulation is one of the fundamental steps, since it allows computation – among other things – of various fundamental values such as the power density (used in thermal hydraulics computations) or fuel burn-up.

The neutron transport simulation is based on the Boltzmann equation [1], which models the neutron population inside the reactor core. Among the various methods allowing its numerical solution, much interest has been devoted in the past few years to the Method of Characterics in unstructured meshes (MOC), since it offers a good accuracy and operates in complicated geometries [2].

In its classical version, the MOC accurately accounts for transport within the regions by means of an analytical integration of the neutron flux along a set of trajectories in directions given by an angular quadrature formula. These trajectories are computed during an initial step of the calculation, which is called the tracking phase. Although much work has been done on tracking issues and many techniques have been proposed to reduce the approximations introduced by the angular quadrature formula [3], few studies have been focused on the discretization errors due to the tracking step used to track the set of trajectories in a given direction [4].

The objective of this work is to palliate the geometrical approximations due to trajectory tracing by properly accounting for (a) the material discontinuities along the trajectories and (b) the transverse variation of the transmission probability, without penalizing the tracking step.

F. Févotte is with the Commissariat à l'Energie Atomique, Centre de Saclay, CEA/DEN/DANS/DM2S/SERMA/LTSD, France. (tel: +33 1 69 08 22 60, e-mail: francois.fevotte@cea.fr).

S. Santandrea is with the Commissariat à l'Energie Atomique, Centre de Saclay, CEA/DEN/DANS/DM2S/SERMA/LTSD, France. (tel: +33 1 69 08 81 78, e-mail: simone.santandrea@cea.fr).

R. Sanchez is with the Commissariat à l'Energie Atomique, Centre de Saclay, CEA/DEN/DANS/DM2S/SERMA/LTSD, France. (tel: +33 1 69 08 54 04, e-mail: richard.sanchez@cea.fr).

This paper is organised as follows: in the next section, we briefly review the Boltzmann equation and the classical Method of Characteristics (MOC). Then we present in section 3 the new macroband technique, while numerical examples are given in the following section. We end with a brief conclusion.

2. Neutron Transport with the MOC

A. The Boltzmann Equation

Before deriving the Boltzmann equation, we have to define the relevant dependant variables. In a general case, seven independent variables are required to describe a neutron population: time t, and coordinates in a 6-dimension phase space

- $\mathbf{r}$: spatial coordinates (3 coordinates);
- v: velocity[1] (1 coordinate);
- $\mathbf{\Omega}$: direction of flight[2] (2 coordinates)

The neutronic population is always seen under a statistic viewpoint, and is represented by the *neutron density distribution* $N(\mathbf{r},v,\mathbf{\Omega},t)$, such that $N(\mathbf{r},v,\mathbf{\Omega},t)dv\,d^3\mathbf{r}\,d^2\mathbf{\Omega}$ is the number of neutrons at time t in a volume element $\left(d^3\mathbf{r},dv,d^2\mathbf{\Omega}\right)$ around point $(\mathbf{r},v,\mathbf{\Omega})$ in the phase space. Although this density distribution is the fundamental dependent variable, most transport problems are formulated in terms of the *angular flux*:

$$\psi(\mathbf{r},v,\mathbf{\Omega},t)=v\,N(\mathbf{r},v,\mathbf{\Omega},t).$$

The materials crossed by the neutron flux are characterized by their macroscopic cross-section Σ. For any interaction of type x, the number of interactions between the neutronic population and the material per unit time and per unit volume can be defined as the *reaction rate*:

$$\tau_x(\mathbf{r},v,\mathbf{\Omega},t)=\Sigma_x(\mathbf{r},v,t)\,\psi(\mathbf{r},v,\mathbf{\Omega},t).$$

The Boltzmann equation is derivated by computing the change in the number of particles between t and $t+dt$ in a volume element in the phase space. The change in this quantity can be attributed to three mechanisms:

1. Streaming of neutrons in and out of the volume element across its surfaces;

2. Collisions that cause neutrons to be absorbed or to be scattered outside of the volume element;

3. Emission of neutrons in the volume element from scattering, fission or external sources.

Derivating these three terms yields the following Boltzmann equation (in which we omitted the variables for the sake of readability):

$$\frac{1}{v}\frac{d\psi}{dt}=\underbrace{-\mathbf{\Omega}\cdot\nabla_{\mathbf{r}}\psi}_{\text{streaming}}-\underbrace{\Sigma_t\psi}_{\text{collisions}}+\underbrace{q}_{\text{sources}}. \qquad (1)$$

In this formulation, Σ_t represents the total cross section of the material, and the source term q comprises both the neutron sources (fission or external sources) and the scattering. The detailed expression of the latter is of no interest for the following.

More details about the derivation of the Boltzmann equation are available in [1].

B. The Method of Characteristics

The Method of Characteristics (MOC) is widely used for transport problems [2],[5]-[7]. It provides a solution for the Boltzmann equation in a geometric domain D:

$$\begin{cases}(\mathbf{\Omega}\cdot\nabla+\Sigma)\psi=q, & (\mathbf{r},\mathbf{\Omega})\in D\times S_N \\ \psi=\beta\psi+\psi_0, & (\mathbf{r},\mathbf{\Omega})\in\partial D\times S_N^-\end{cases} \qquad (2)$$

where $\psi(\mathbf{r},\mathbf{\Omega})$ represents the angular flux at position $\mathbf{r}$ in direction $\mathbf{\Omega}$, $\Sigma(\mathbf{r})$ represents the total cross-section and $q(\mathbf{r},\mathbf{\Omega})$ is the emission density of the neutron sources. β is an albedo operator on the domain boundary, and ψ_0 represents an angular flux entering through the boundary.

Equation (2) is simply a reformulation of the Boltzmann equation (1), in a time-independent fashion, and in which the energy E (or velocity v) has been discretized in a multigroup formalism, and the direction of flight $\mathbf{\Omega}$ is discretized in an S_N quadrature formula. Since it does not affect the present work, we dropped the energy variable dependance for the sake of readability.

In the method of characteristics, the spatial discretization is achieved by assuming that the geometric domain is composed of unstructured homogeneous regions, and introducing approximated representations for the dependant variables within the regions. First, a region-wise flat spatial representation is used for the source term and the cross-sections:

$$\begin{cases}q(\mathbf{r},\mathbf{\Omega})=q_i(\mathbf{\Omega}), \\ \Sigma(\mathbf{r})=\Sigma_i,\end{cases}\quad \mathbf{r}\in\text{region }i. \qquad (3)$$

Integrating equation (2) on a straight trajectory t of direction $\mathbf{\Omega}$ crossing region i yields the following equations:

---

[1] We coud also have used the neutron energy E instead of its velocity.

[2] We could also use a single velocity vector $\mathbf{v}$ in place of both variables v and $\mathbf{\Omega}$

$$\psi_i^+(t) = e^{-\Sigma_i R_i(t)} \psi_i^-(t) + \frac{1 - e^{-\Sigma_i R_i(t)}}{\Sigma_i} q_i(\mathbf{\Omega}), \quad (4)$$

$$\psi_i(t) = \frac{\psi_i^-(t) - \psi_i^+(t)}{\Sigma_i R_i(t)} + \frac{q_i(\mathbf{\Omega})}{\Sigma_i}, \quad (5)$$

with the notations of fig. 1: $\psi_i^\pm(t)$ are the angular fluxes entering (-) and exiting (+) region i along the trajectory t, $\psi_i(t)$ is the average angular flux along the trajectory within the region, and $R_i(t)$ is the chord length of the trajectory within the region. In equation (4), the term $e^{-\Sigma_i R_i(t)}$ represents a transmission probability for the angular flux across the region.
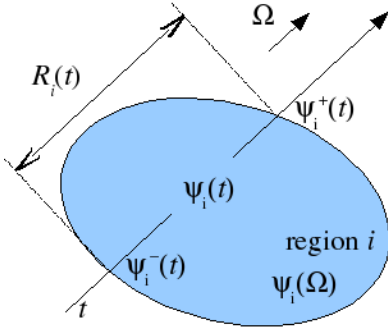
Fig. 1. Transmission of the angular flux across a region along a characteristic line.

Thus, starting with a given initial boundary condition and repeatedly applying equations (4) and (5) on a line intersecting the geometric domain, we can compute the average angular fluxes along each line segment intersecting an homogeneous region.

In most practical applications of the MOC, a mesh is defined over the plane transverse to the direction of propagation $\mathbf{\Omega}$. The region-averaged angular flux $\psi_i(\mathbf{\Omega})$, is then computed using an integration quadrature formula based on the trajectories at the center of the transverse mesh cells:

$$\psi_i(\mathbf{\Omega}) = \frac{\sum_k \psi_i(t_k) \Delta_k}{\sum_k \Delta_k}, \quad (6)$$

where t_k is the trajectory at the center of the k'th mesh cell. We can imagine each trajectory t_k to be lying within a *trajectory band* of cross sectional area Δ_k (fig. 2), and the summation is done over all the trajectory bands k for which t_k crosses the considered region i.

Usually, the transverse mesh is defined with a constant step Δ, so that $\forall k, \Delta_k = \Delta$. In the following, we will refer to Δ as the *tracking step*.
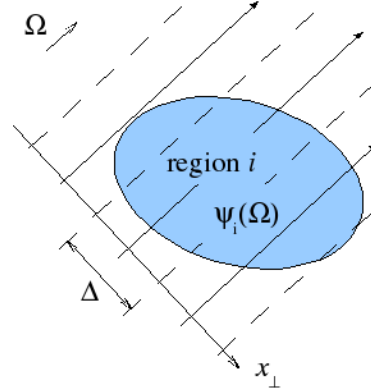

Fig. 2. Classical transverse mesh.

3. The Macroband Method

A. Tracking-Related Issues

Equation (6) is only valid under a few assumptions:

(a) the angular flux is constant across each transverse mesh cell;

(b) the transmission probability of the angular flux across a region intersecting the trajectory band can be approximated by the value of the transmission for the trajectory at the center of the band.

However, both assumptions are only approximately verified for large values of the tracking step Δ and thus entail a loss of accuracy on the solution. This work focuses on assumption (b), which fails for large values of the tracking step for two reasons:

- *material discontinuities*: numerically, the intersection between a region and a band only occurs when the middle trajectory intersects the region. Thus partially inserted regions may not be accounted for in a band, and the transmission is computed as though the region was not there. For example, this phenomenon occurs in fig. 2, where the region intersects the topmost band, but is not crossed by the corresponding trajectory.

- *transverse variation of the chord length*: in equation (4), the transmission probability is computed using only the chord length at the middle of the band, although this chord length usually varies transversally across the band.

As a consequence of these approximations, rather small tracking steps have to be used in order to obtain accurate results with the method of characteristics. Moreover, the lack of accounting for material discontinuities not only affects the precision of the

3

calculation, but also results in a non uniform convergence with the tracking step Δ. The main aim of this work is to propose a technique to avoid such effects in order to eventually be able to increase the tracking step (and thus gain computing resources) without loss of accuracy on the solution.

B. Avoiding Material Discontinuities

To eliminate the oscillations and achieve uniform convergence one can project all the material discontinuities over the transverse direction and integrate within each two consecutive projections.

Moreover, because the integrand is now continuous, the transverse integration of equation (6) can be done using a more accurate Gauss-Legendre (GL) quadrature [3]. Unfortunately, the projection of discontinuities usually produces a transverse mesh with a large number of small mesh cells that, not only does not require GL quadrature, but that is too precise and onerous for routine applications. Even when limiting the projection of discontinuities to each cell of an assembly, there is no notable advantage on using a GL quadrature [4]. Besides, this latter solution introduces a fair amount of numerical dispersion for the transverse flux when passing from one cell to the following.

In this work, we propose a technique that uses *macrobands* to locally project the discontinuities so as to minimize the presence of very small quadrature steps. This is done as follows:

1. For each direction Ω in the angular quadrature formula, we define a constant-step transverse quadrature mesh of cell width Δ. This mesh defines *macrobands* of direction Ω that cover the entire domain (Fig. 3).

2. Each macroband is split into *sections*, so that the interfaces between two consecutive sections follow the region boundaries (Fig. 4).

3. The projection of material discontinuities is done locally within each section, and leads to the decomposition of each section in one or more continuous *sub-bands* (Fig. 4).

4. Flux propagation along each sub-band is calculated using a transmission equation (either the classical transmission equation (4) or a more advanced equation that shall be discussed in the following section).

5. At section interfaces, the upstream and downstream sections may not have the same number of sub-bands, so that the fluxes exiting the upstream sub-bands have to be redistributed into the fluxes entering the downstream sub-bands (Fig. 5).

The flux redistribution at section interfaces is necessary to ensure neutron conservation and reduce as much as

possible the numerical dispersion introduced at the section interfaces. Assuming that the upstream flux $\psi_{k'}^{upstr}$ is constant within the homogeneous sub-band k' of the upstream section, we can compute the downstream fluxes using the following formula:

$$\psi_k^{downstr} = \sum_{k'} \frac{\Delta_{kk'}}{\Delta_k} \psi_{k'}^{upstr}, \qquad (7)$$

where the sum in k' is done over all the sub-bands of the upstream section, Δ_k represents the width of downstream sub-band k, and $\Delta_{kk'}$ denotes the length of intersection of downstream sub-band k with upstream sub-band k' (fig. 5).
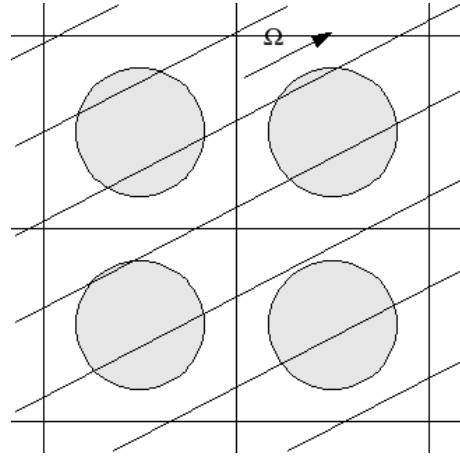

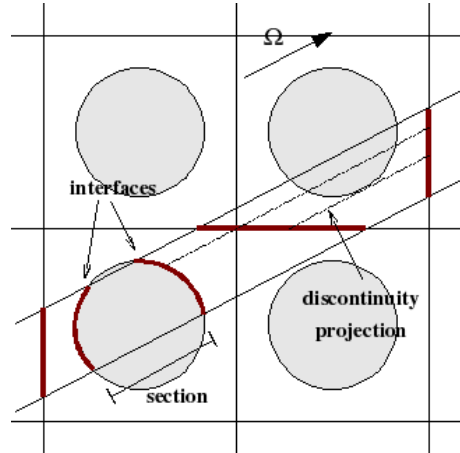Fig. 3. Transverse mesh defining macrobands on a cluster of simplified PWR fuel cells.

Fig. 4. Example of sections and local projection of material discontinuities in a cluster of simplified PWR fuel cells.

C. Improved Transmission Probabilities

The classical transmission equation (4) only uses the middle trajectory to compute a transmission probability. However, for consistency with the
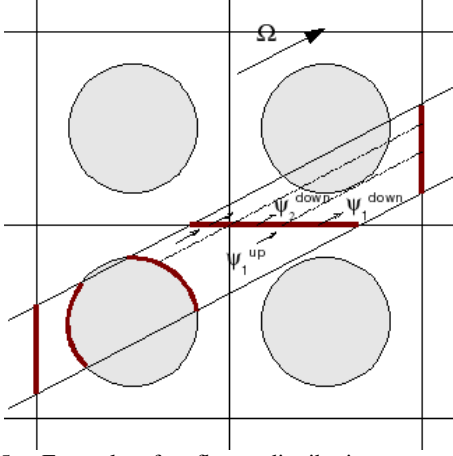
4

Fig. 5. Example of a flux redistribution at a section interface in a cluster of simplified PWR fuel cells.

piecewise constant approximation for the angular flux on the transverse direction, the transmission equation should be averaged over all trajectories in the trajectory band:

$$\psi_{i,k}^+ = T_{i,k}\ \psi_{i,k}^- + \frac{1-T_{i,k}}{\Sigma_i} q_i(\boldsymbol{\Omega}), \qquad (8)$$

where the notations are consistant with those of equation (4), with i and k respectively indexing the region crossed and the considered band. $T_{i,k}$ is the averaged transmission coefficient across region i within band k:

$$T_{i,k} = \frac{\displaystyle\int_{x_\perp \in I_k} e^{-\Sigma_i R_i(x_\perp)}\ dx_\perp}{\displaystyle\int_{x_\perp \in I_k} dx_\perp}, \qquad (9)$$

where the integration is done over the transverse extension of band k, and $R_i(x_\perp)$ represents the chord length within region i for the trajectory at transverse abscissa $x_\perp$.

Because our local projection of the discontinuities ensures that there are no discontinuities within the trajectories paths in a sub-band, an approach could consist of using a low-order Gauss-Legendre quadrature to evaluate integral (9). However such a method would significantly increase the amount of trajectory storage and, more importantly, the numerical effort during the sweep. Instead, we have chosen to use a few-term Taylor expansion for the exponential and write:

$$T = e^{-\Sigma \overline{R}} \sum_{p=1}^{n} \alpha_p\ \Sigma^p, \qquad (10)$$

where we dropped indices i and k for the sake of readability. n is the Taylor expansion order, and $\overline{R}$ is the mean chord length for the band within the region, and

$$\alpha_p = \frac{(-1)^p}{p!\,\Delta} \int_{x_\perp \in I_k} \left[R(x_\perp) - \overline{R} \right] dx_\perp. \qquad (11)$$

The values of $\overline{R}$ and α_p can be computed using a Gauss-Legendre quadrature during the tracking phase, so that formula (10) only adds a few operations to the track sweep.

4. Numerical Results

We have implemented this new transverse quadrature technique in the characteristic solver of the APOLLO2 code [6], and present here some of the results obtained for different geometry configurations.

When not otherwise specified, the results presented below used a Taylor expansion of order $n = 5$ in equation (10).

Because the macrobands in our technique are composed of heterogeneous sections and each section may contain more than one track, to establish a fair comparison with the approximation used in the classical MOC we convert our tracking step Δ into an *effective tracking step*:

$$\Delta_{eff} = \frac{\Delta}{n_{sb}},$$

where n_{sb} is the average number of sub-bands within a section. In other words, Δ_{eff} is the average width of the homogeneous sub-bands. In all the following results, we use this effective tracking step Δ_{eff} to compare the new technique with a classical MOC with step Δ.

A. Convergence

We consider first the simple fuel cell in Fig. 6a with a uniform source in the moderator. The relative errors in the absorption rate versus the tracking step (Δ for classical MOC and Δ_{eff} for the new technique) are given in Fig. 6b. We observe that classical MOC exhibits nonuniform convergence, as a result of partial region intersections with trajectory bands. On the other hand, the new technique converges monotonously even for large tracking steps.
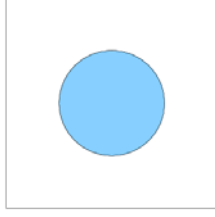
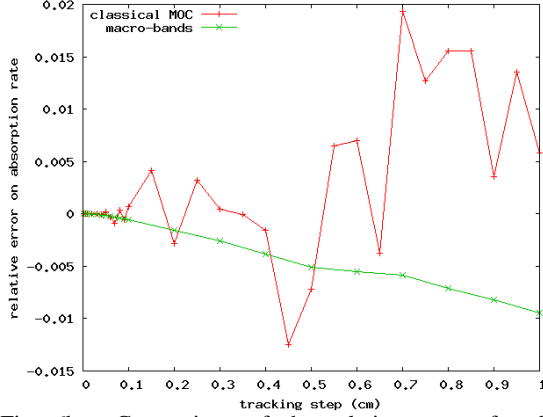Fig. 6a. Geometry of a simplified PWR fuel cell.

Fig. 6b. Comparison of the relative errors for the integrated absorption rate versus tracking step on a simplified PWR fuel cell. The reference is a classical MOC with $\Delta = 0.005\, mm$.

B. Accuracy

Fig. 6b also shows that for the same transverse band size the macroband technique is up to six times more accurate than the classical MOC. Conversely, for a given precision, the macroband method allows for a tracking step up to five times larger than the classical MOC. For example, to obtain the same precision as in a regular MOC calculation with $\Delta = 0.2\, mm$, the tracking step with macrobands could be increased up to $\Delta_{eff} = 1\, mm$.

These results scale to larger cases. Figures 7 and 8 show a comparison between the classical and the new transverse quadrature techniques over domains with about 500 regions, respectively for a typical RBMK cell and a typical rodded PWR assembly. To avoid compensation errors by full domain averaging, we compared here the maximum relative error in the absorption rate per region. As shown in the figures, error compensation due to the large number of regions makes somewhat smoother the convergence of the classical MOC. Regardless, the gain in precision with the macroband technique is still significant. For example, a precision of 1% can be obtained with $\Delta_{eff} = 0.1\, mm$, whereas the regular MOC requires $\Delta = 0.025\, mm$ for the same precision.
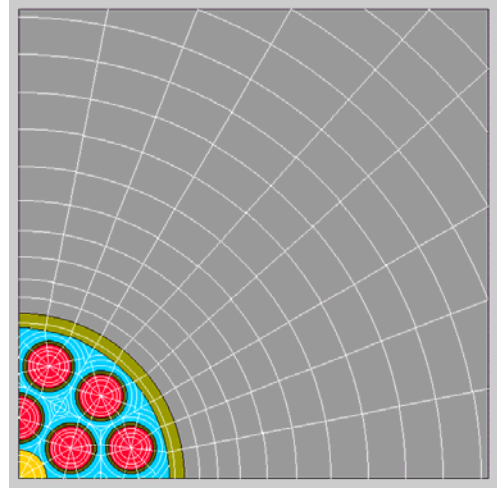

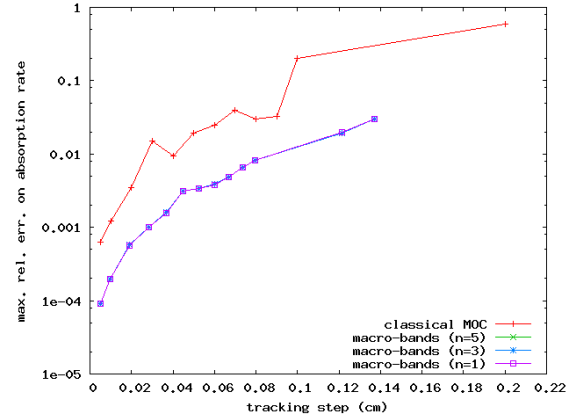Fig. 7a. Geometry of a fourth of RBMK cell.

Fig. 7b. Comparison of the maximum relative errors for the absorption rate per region versus tracking step on a typical RBMK cell. The reference is a classical MOC with $\Delta = 0.005\, mm$.

For the PWR assembly calculation (fig. 8b), one observes that the averaged number of homogeneous sub-bands n_{sb} per section increases with the tracking step Δ. Thus, there is a limit value of Δ beyond which the effective tracking step Δ_{eff} stagnates (and even decreases) and there is no further improvement of the results.

A final word regarding the sensitivity of the results with respect to the order n of the Taylor expansion in Equation (10): figures 7b and 8b show that there is a negligible gain when increasing n. Therefore, one could reduce n to 1 – and even 0 – with no appreciable loss in precision. The implication is that, when there is a large number of regions in the geometry domain, the main cause for the error of the classical transverse quadrature is due to the neglect of a correct treatment for regions discontinuities within track bands.
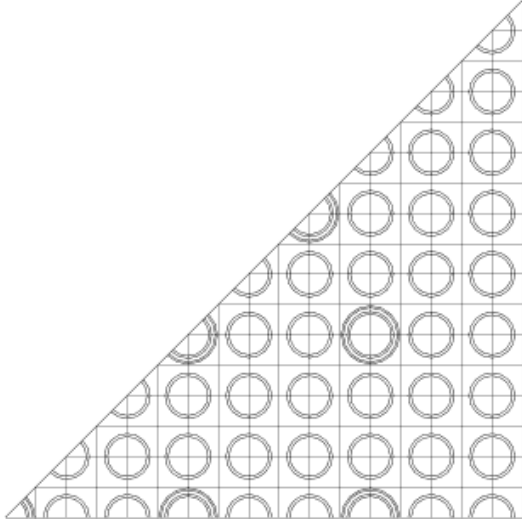
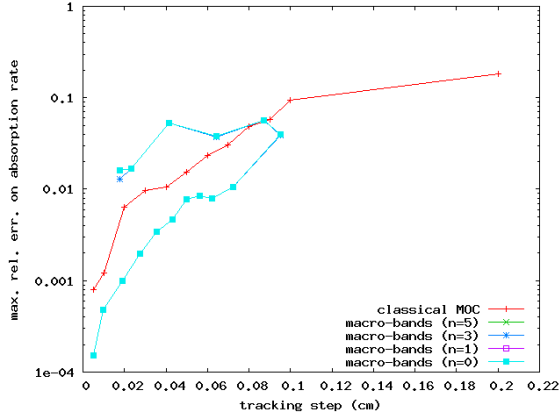Fig. 8a. Geometry of an eighth of rodded PWR assembly.

Fig. 8b. Comparison of the maximum relative errors for the absorption rate per region versus tracking step on a typical rodded PWR assembly. The reference is a classical MOC with $\Delta = 0.005\,mm$.

C. Computing Time

Due to the lack of optimization in the implementation of the new transverse quadrature, a direct comparison of computing times with the classical MOC is unfeasible at the time of this writing. Nevertheless, we may compare their algorithmic complexities, both in terms of number of operations and tracking storage requirements. As far as the sweeping is concerned, the move to the macroband technique affects only the treatment of the transmission equation.

The number of arithmetic operations and the size of the tracking data required per track sweep for the macroband and the classical tracking techniques, based respectively on Eq. (4) and on Eqs. (8) and (10), are compared in Table I.

TABLE I
ALGORITHMIC COMPLEXITIES FOR THE CLASSICAL MOC AND THE MACROBAND METHOD

Type of Operation	exp	×	+	storage
Classical MOC	1	2	2	1
Macrobands ($n \neq 0$)	1	$3+n+r$	$2+n$	$1+n+2r$
Macrobands ($n = 0$)	1	$2+r$	2	$1+2r$

r represents the average cost for flux repartition at section interfaces

Because of its dependence on the regions shape and distribution throughout the domain, we are unable to predict the exact value for the average computing cost r for flux redistribution. However, we can evaluate it *a posteriori*, for a particular problem as:

$$r = \frac{n_{sb}}{n_{reg}},$$

where n_{sb} is the average number of sub-bands within a section, and n_{reg} is the average number of regions crossed by a sub-band. A conservative value for the RBMK cell calculation shown in figure 4 is $r \approx 0.6$. This implies that with a first-order Taylor expansion the new technique requires roughly 2.3 times the amount of operations and 3.2 times the amount of storage needed by the classical MOC with the same tracking step Δ. For a 0th order Taylor expansion (i.e. when approximating the transmission probability using only the average chord length), the only additional cost for the macrobands is due to the flux repartition at section interfaces.

5. Conclusion

We have developed and implemented a new tracking technique for the method of characteristics that accounts for material discontinuities and uses a semi-analytical transverse quadrature formula. The observed gain in precision compared to the classical MOC tracking confirms that it is the low precision of the classical transverse integration that severely limits the accuracy of the MOC.

Our numerical examples show that macroband transverse quadrature gives equivalent results than the classical MOC with tracking steps up to 5 times greater. It also guarantees monotonous convergence, even for large values of the tracking step. A comparison of numerical cost and tracking storage requirements shows promise that, with a properly optimized implementation, the macroband method can be nearly twice as fast as the classical MOC.

7

Still, there remains the error introduced by the piecewise constant approximation for the transverse variation of the angular flux. In future research we intend to investigate the use of a piecewise linear flux transverse expansion. The combination of this improved flux expansion with the macroband tracking technique introduced in this work has potential for a further increase of the tracking step for a given accuracy.

References

[1] E. E. Lewis and Computational Methods of Neutron Transport, American Nuclear Society, LaGrange Park, Illinois USA (1993), chapter 1.

[2] M. J. Halsall, *"CACTUS, a Characteristics Solution to the Neutron Transport Equations in Complicated Geometries"*, AEEW-R 1291, Atomic Energy Establishment, Winfrith, UK (1980).

[3] R. Sanchez, L. Mao and S. Santandrea, *"Treatment of Boundary Conditions in Trajectory-Based Deterministic Transport Methods"*, Nuclear Science and Engineering, Vol. 140, pp. 23-50 (2002).

[4] A. Yamamoto, M. Tabushi, N. Sugimura and T. Ushio, *"Non-Equidistant Ray Tracing for the Method of Characteristics"*, in Proc. M&C 2005, Avignon, France (2005).

[5] S. G. Ho and N. Z. Cho, *"CRX, a Code for Rectangular and Hexagonal Lattices Based on the Method of Characteristics,"* Annals of Nuclear Energy, Vol. 25, pp. 547-565, 1998.

[6] R. Sanchez, J. Mondot, Z. Stankovski, A. Cossic and I. Zmijarevic, *"APOLLO2: a User-Oriented, Portable, Modular Code for Multigroup Transport Assembly Calculations,"* Nuclear Science and Engineering, Vol. 100, pp. 352, 1988.

[7] K. S. Smith and J. D. Rhodes, *"CASMO-4 Characteristics Methods for Two-Dimensional PWR and BWR Core Simulations,"* Trans. Am. Nucl. Soc., Vol. 83, pp. 294-296, 2000.